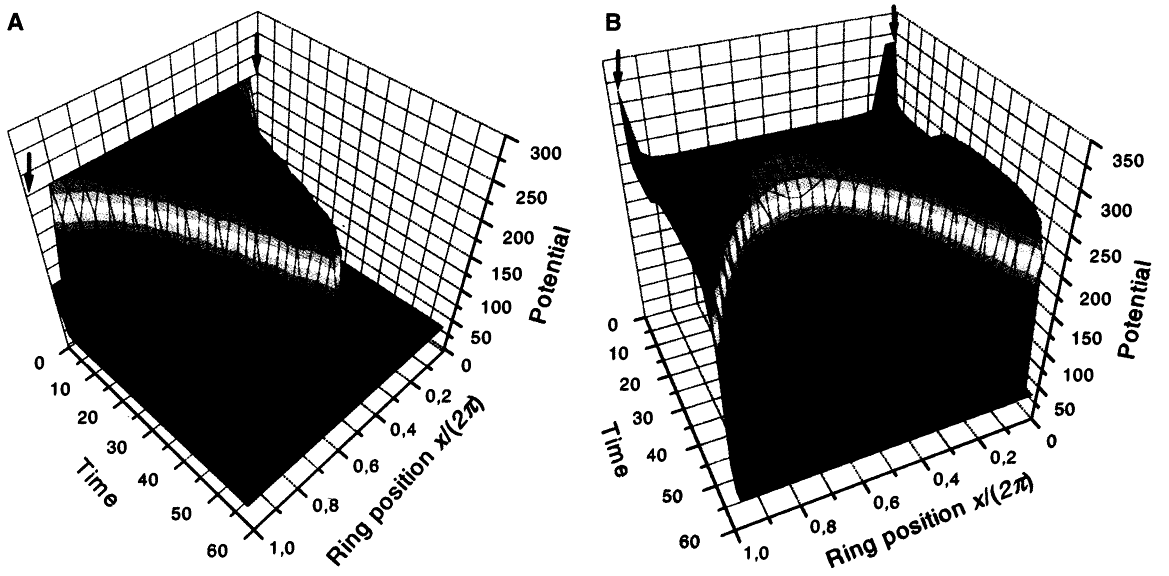

Fig. 4. Simulated passive-active transitions with the reaction-migration Eq. 2 in the bistable regime: periodic boundary conditions (corresponding to a ring), with perturbation applied in the region. 0 = 2π ($i_{\mathrm{real}} = \Sigma_{i=1}^{3} a_i u^i$, a_1 = 5.5932, a_2 = −0.04725, a_3 = 10^{-4}; E = 233.5, R = 1.5, κ = 0.057, C = 1.) All quantities are given in dimensionless units. The passive state corresponds to a potential u of 230, and the active state corresponds to a potential u of 30. (**A**) Local triggering, with u locally lowered by 126 over an angle of 30° in the initial conditions. (**B**) Remote triggering, with u locally increased by 250 over a 45° angle in the initial conditions (plot starts t = 0.2 s).

4A), whereas the opposite perturbation triggered the transition 180° away (Fig. 4B), in complete agreement with the experiment.

The remote triggering of electrochemical reaction fronts provides a direct experimental demonstration of the nonlocal nature of migration coupling (*5*). It can be easily rationalized in terms of the coupling function H (Fig. 3), which is positive for small distances (thus enabling front propagation) but negative further away, allowing a local perturbation with the "wrong" sign to manifest itself at a remote distance, where its sign is reversed by the coupling. Nonlocal phenomena are obviously not restricted to bistability but are expected to manifest themselves also for more complex local dynamics [compare with (*12*, *13*)].

The apparently "instantaneous" coupling observed arises from the slow time scale of the reaction (about 0.1 s for the removal of the passivating OH layer), whereas the electric field effects spread with the velocity of light (less than 10^{-9} s across the system). Hence, nonlocal effects, such as remote triggering, are expected whenever a very fast coupling occurs in a system with slow local dynamics. This includes not only electrochemical reactions but also biochemical processes coupled by electric field effects.

References and Notes

1. R. Kapral and K. Showalter, Eds., *Chemical Waves and Patterns* (Kluwer Academic, Dordrecht, Netherlands, 1995).
2. Special issue on Wave Patterns in Chemical and Biological Systems, H. L. Swinney and V. I. Krinsky, Eds., *Physica D* **49** (no. 1/2) (1991).
3. A. T. Winfree, *When Time Breaks Down* (Princeton Univ. Press, Princeton, NJ, 1987).
4. J. D. Murray, *Mathematical Biology* (Springer-Verlag, Berlin, 1990).
5. K. Krischer, in *Modern Aspects of Electrochemistry*, vol. 32, B. E. Conway, J. O. Bockris, R. White, Eds. (Plenum, New York, in press).
6. P. Strasser, M. Lübke, F. Raspel, M. Eiswirth, G. Ertl, *J. Chem. Phys.* **107**, 979 (1997).
7. G. Flätgen and K. Krischer, *Phys. Rev. E* **51**, 3997 (1995); *J. Chem. Phys.* **103**, 5428 (1995).
8. J. Christoph, thesis, Freie Universität Berlin (1999).
9. P. Grauel, J. Christoph, G. Flätgen, K. Krischer, *J. Phys. Chem. B* **102**, 10264 (1998).
10. J. Christoph, R. Otterstedt, M. Eiswirth, N. I. Jaeger, J. L. Hudson, *J. Chem. Phys.*, in press.
11. N. Mazouz, G. Flätgen, K. Krischer, *Phys. Rev. E* **55**, 2260 (1997).
12. J. C. Sayer and J. L. Hudson, *Ind. Eng. Chem. Res.* **34**, 3246 (1995).
13. Z. Fei, R. G. Kelly, J. L. Hudson, *J. Phys. Chem.* **100**, 18986 (1996).

29 December 1998; accepted 3 March 1999

Electrodeposited Ceramic Single Crystals

Jay A. Switzer,* Mark G. Shumsky, Eric W. Bohannan

Single-crystal films are essential for devices because the intrinsic properties of the material, rather than its grain boundaries, can be exploited. Cubic bismuth oxide has the highest known oxide ion mobility, which makes it useful for fuel cells and sensors, but it is normally only stable from 729° to 825°C. The material has not been previously observed at room temperature. Single-crystal films of the high-temperature cubic polymorph of bismuth oxide were epitaxially electrodeposited from an aqueous solution onto single-crystal gold substrates. The 35.4 percent lattice mismatch was accommodated by forming coincidence lattices in which the bismuth oxide film was rotated in relation to the gold substrate. These results provide a method for producing other nonequilibrium phases that cannot be accessed by traditional thermal processing.

Electrodeposition can be used to produce nonequilibrium materials and architectures that cannot be accessed by traditional thermal processing. Nonequilibrium crystal structures can be stabilized by producing nanometer-scale crystallites or by epitaxially depositing the material onto a template with a crystal structure similar to the one desired. We have previously used electrodeposition to produce nonequilibrium layered nanostructures and superlattices of metal oxides that showed quantum confinement effects (*1*–*6*). Here, we show that single-crystal films of the high-temperature cubic polymorph of bismuth oxide (δ-Bi_2O_3) can be epitaxially electrodeposited onto cubic single-crystal Au substrates. The system achieves epitaxy by forming coincidence lattices in which the δ-Bi_2O_3 overlayer is rotated in relation to the

---

University of Missouri–Rolla, Department of Chemistry and Graduate Center for Materials Research, Rolla, MO 65409–1170, USA.

*To whom correspondence should be addressed. E-mail: jswitzer@umr.edu

Au single-crystal substrate. There is great interest in δ-Bi_2O_3 for use in fuel cells, oxygen sensors, and oxygen pumps because it has the highest oxide ion mobility of any known material (*7, 8*). Unfortunately, the cubic structure is only stable from 729°C to the melting point at 825°C. The conductivity drops by over three orders of magnitude at temperatures less than 729°C, when the material transforms to the monoclinic (α-Bi_2O_3) form. Furthermore, the volume change that is associated with the δ → α phase transition produces cracking and severe deterioration of the material, and the oxide tends to reduce to Bi metal at the high temperatures and reducing conditions of conventional fuel cells. The cubic structure can be stabilized by the addition of rare-earth metal ions, but the conductivity drops by about two orders of magnitude. The single-crystal δ-Bi_2O_3 films that we produced are not doped, and they are stable at room temperature.

The underpotential deposition (UPD) of monolayers of metals onto single-crystal surfaces has been studied extensively (*9*), yet there has been little work on the deposition of single-crystal films with thicknesses in the micrometer range. Budevski and co-workers have shown that "quasi-perfect" single crystals of Ag can be electrodeposited onto single-crystal Ag substrates (*10*). Moffat has used electrodeposition to produce single-crystal Cu-Ni strained-layer superlattices on Cu(100) (*11*). Lincot *et al.* have demonstrated that epitaxial CdTe films can be electrodeposited onto InP(111) single crystals in a one-step process from aqueous solution (*12*). Hodes, Rubinstein, and co-workers have produced quantum dots of Cd(Se,Te) in the 5-nm range on evaporated Au(111) films (*13*), and Penner and co-workers have used a hybrid electrochemical-chemical method to synthesize epitaxially oriented nanocrystallites on a graphite surface (*14*).

The δ-Bi_2O_3/Au epitaxial system is challenging because of the large lattice mismatch between δ-Bi_2O_3 and Au. The δ-Bi_2O_3 that we deposited has a lattice parameter of 0.5525 ± 0.0001 nm (in comparison with 0.4079 nm for Au), resulting in a lattice mismatch, $(a_{\text{film}} - a_{\text{substrate}})/a_{\text{substrate}}$, of 35.4%. The crystal structures of δ-Bi_2O_3 and Au are shown in Fig. 1. Both materials have a face-centered–cubic (fcc) Bravais lattice. The Au has a simple structure, with one Au atom on each fcc lattice site, whereas the δ-Bi_2O_3 has a distorted fluorite structure with one-quarter of the O atoms missing. The O vacancies are randomly distributed to produce the fcc structure. Neutron diffraction studies have shown that the O atoms are displaced from the standard positions (1/4, 1/4, 1/4) of the fluorite structure to form a highly disordered O sublattice (*15, 16*). The high oxide mobility of the material has been attributed to the disorder on the O sublattice (*17, 18*).

We electrodeposited the black δ-Bi_2O_3 films at 65°C at an anodic current density of 5 mA/cm^2 from an aqueous solution of 0.1 M $Bi(NO_3)_3$, 0.25 M tartaric acid, and 2.5 M KOH. Our experimental results suggest that the initial product in the electrochemical oxidation is Bi(V) oxide, which loses O to produce crystalline δ-Bi_2O_3. If the deposition is run at temperatures less than 50°C, a red amorphous film is produced, which gives a positive iodometric test for Bi(V). Rietveld refinement of the x-ray diffraction pattern of crystalline powder produced at 65°C shows that the material has the high-temperature fcc structure. Films deposited onto stainless steel and glassy carbon have a near-random orientation of nanometer-scale crystallites with a 70- to 80-nm coherence length, whereas films deposited onto the (110), (100), and (111) surfaces of single-crystal Au have a strong

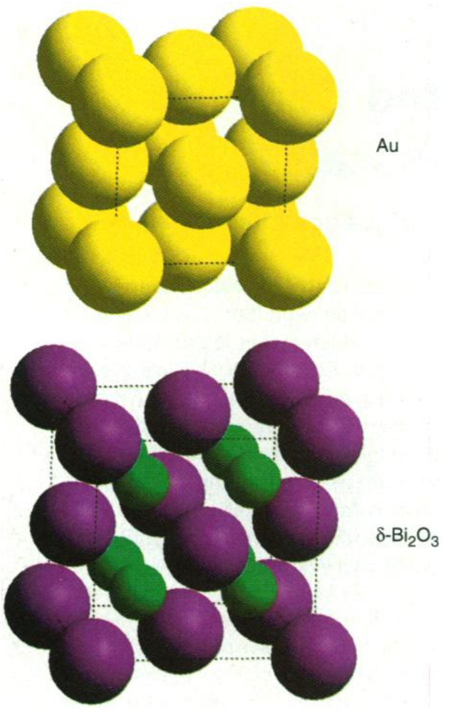

Fig. 1. Crystal structures of Au and δ-Bi_2O_3. Both materials have an fcc Bravais lattice and an *Fm*3*m* space group. The δ-Bi_2O_3 has a distorted fluorite structure with Bi atoms (purple) at (0, 0, 0) and O atoms (green) at 75% of the ±(1/4, 1/4, 1/4) sites. Oxygen vacancies are randomly distributed to produce the fcc structure. The δ-Bi_2O_3/Au lattice mismatch is 35.4%.

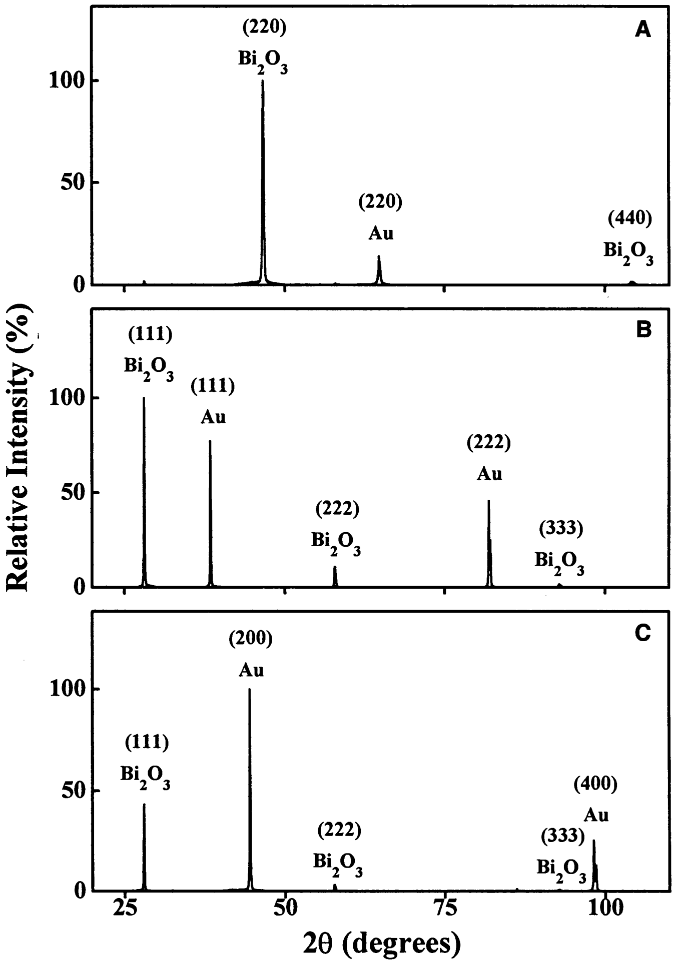

Fig. 2. Bragg-Brentano x-ray diffraction scans probing the out-of-plane orientation of δ-Bi_2O_3 films deposited onto (**A**) Au(110), (**B**) Au(111), and (**C**) Au(100) single-crystal substrates. The δ-Bi_2O_3 films were 1.7 μm thick, and the Au crystals had a 1-cm diameter. The x-ray radiation was Cu Kα. The δ-Bi_2O_3 film followed the orientation of the Au(110) and Au(111) crystals but grew with a (111) orientation on the Au(100) single crystal.

out-of-plane and in-plane orientation with very high structural perfection.

The out-of-plane (that is, perpendicular to the substrate) orientation of the films was probed by x-ray diffraction in the Bragg-Brentano (θ-θ, where θ is the diffraction angle) configuration. Plots of relative intensity versus 2θ for films deposited onto the (110), (111), and (100) surfaces of Au are shown in Fig. 2. The diffracted intensity from the δ-Bi$_2$O$_3$ films was very high. Although the films were only 1.7 μm thick, the intensity of the peaks from δ-Bi$_2$O$_3$ was comparable to those from the single-crystal Au. The films on the (110) and (111) substrates followed the out-of-plane orientation of the Au substrate. The film on Au(110) shows strong (220) and (440) peaks, and the film on Au(111) shows strong (111), (222), and (333) peaks. The (110) reflection is systematically absent from the x-ray pattern for the (110)-oriented film because this reflection is symmetry forbidden for the fcc structure. In contrast to the (110) and (111) samples, the film grown on Au(100) has a different out-of-plane orientation than the single-crystal substrate. The substrate has a (100) orientation, and the film has a (111) orientation. Rocking (ω) curves for films on the (110), (111), and (100) Au substrates had full width at half maximum values of 3.2°, 2.8°, and 3.7°, respectively, indicating that the films had a slight mosaic spread (that is, composed of blocks that are slightly misoriented).

The in-plane (that is, parallel with the substrate) orientation of the films was probed by azimuthal (ϕ) x-ray scans. Azimuthal scans are two-dimensional sections at a fixed tilt angle (χ) of a three-dimensional x-ray pole figure. They show the in-plane orientation of the film in relation to the substrate. For example, for the film grown on the Au(110) substrate, the scan was performed by selecting $2\theta = 32.39°$, which corresponds to the (200) reflection for δ-Bi$_2$O$_3$. Because this reflection was not observed in the θ-θ scan, no intensity was observed at the detector until the sample was tilted. If the sample is tilted 45° (the angle between the [100] and [110] directions) and rotated through the azimuthal angle, the (200) reflection is brought into the Bragg condition with twofold symmetry if the sample has a (110) in-plane orientation. The azimuthal scans are shown as polar plots in Fig. 3 to accentuate the symmetry of the overlayer. The peak intensity provides a quantitative measure of the degree of alignment. A sample with random in-plane orientation would show a ring in the polar azimuthal plot. The simplest azimuthal scan is shown in Fig. 3A for the film grown on the (110) substrate. Both δ-Bi$_2$O$_3$ and Au show the expected twofold symmetry for the (110) orientation, but the film peaks are rotated 90° in relation to the substrate peaks. The in-plane orientation is very strong; less than 1 volume % of the film does not have this orientation. The azimuthal scan for the film grown on the (111) substrate in Fig. 3B shows an approximate threefold symmetry, but each lobe of the cloverleaf is split into two lobes that are rotated ±8.9° relative to the peaks for the Au substrate. This film may consist of misoriented microdomains, with defects such as stacking faults at the domain boundaries. The azimuthal scan for the (111)-oriented δ-Bi$_2$O$_3$ on the Au(100) substrate in Fig. 3C shows an apparent 12-fold symmetry. In this case, the δ-Bi$_2$O$_3$ peaks are rotated 0° and ±30° in relation to the expected Au(100) fourfold pattern. The δ-Bi$_2$O$_3$ films are rotated in relation to the substrate for all three orientations because of the large lattice mismatch.

On the basis of the 35.4% lattice mismatch of the system, which was calculated by comparing the lattice parameters of the two materials, one would not expect δ-Bi$_2$O$_3$ to grow epitaxially on Au. However, it is possible to construct coincidence lattices by rotating the δ-Bi$_2$O$_3$ film in relation to the Au substrate. Interface models that are consistent with the θ-θ and azimuthal x-ray scans are shown in Fig. 4. The simplest model is that of Bi$_2$O$_3$(110) on the Au(110) surface (Fig. 4A). Because (i) the spacing between Au atoms along the [100] direction is 0.4079 nm, (ii) the spacing of Bi atoms along the [110] direction in Bi$_2$O$_3$ is 0.3907 nm, and (iii) the [110] and [100] directions are orthogonal, a (1×1)Bi$_2$O$_3$(110)[110]//(2×1)Au(110)[100] coincidence lattice with a −4.2% mismatch can be produced by rotating the Bi$_2$O$_3$ 90° in relation to the Au substrate. Because of the relatively low symmetry and packing density of the (110) surface, there is only one way the overlayer can be placed on the Au, and only the 90° rotation is observed in the azimuthal scan. The entire δ-Bi$_2$O$_3$ film shows single-crystal x-ray diffraction, both parallel and perpendicular to the Au single-crystal surface. Epitaxial growth on the (111) surface is more complex because this surface is highly symmetrical and closely packed, and there are several possible epitaxial relations. The (4×4)Bi$_2$O$_3$(111)//$(\sqrt{31} \times \sqrt{31}\ R8.9°)$Au(111) interface model shown in Fig. 4B is consistent with the rotation (*R*) of ±8.9° of the Bi$_2$O$_3$ in relation to the Au that we observed in the x-ray azimuthal scans. The mismatch for this overlayer is only −2.7%. Epitaxy was achieved on the Au(100) surface by growing the Bi$_2$O$_3$ with a (111) out-of-plane orientation and rotating the overlayer 0° and ±30° in plane in relation to the Au. The Bi$_2$O$_3$(111)[121]//Au(100)[100] coincidence lattice shown in Fig. 4C, which is consistent with this observed rotation, has a mismatch of −4.2%.

Electrodeposition is not only a simple and inexpensive method to produce ceramic materials, as we have shown previously (*1–6, 19–23*), but it can also produce epitaxial single crystals with high structural perfection

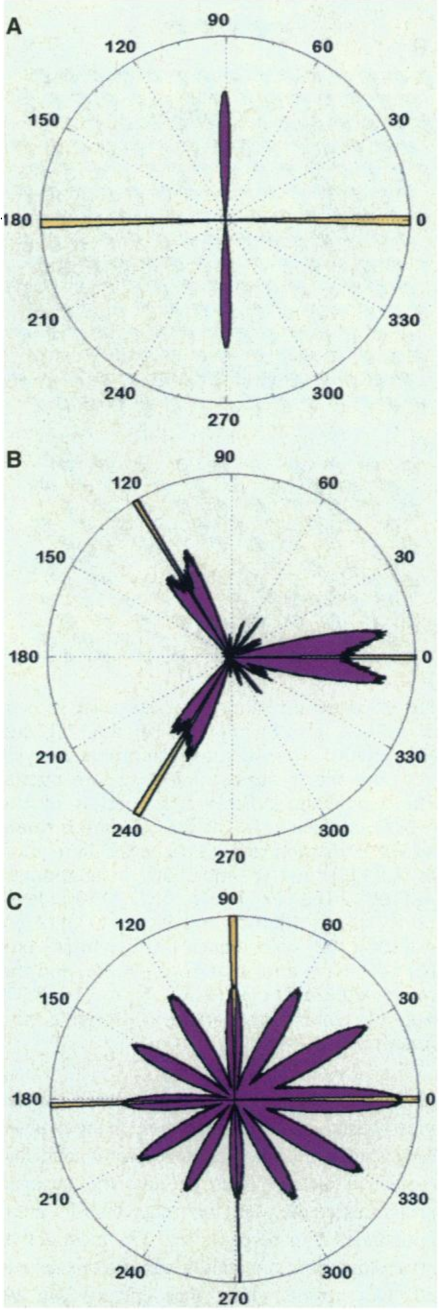

Fig. 3. Azimuthal x-ray diffraction scans probing the in-plane orientation of δ-Bi$_2$O$_3$ films deposited onto (**A**) Au(110), (**B**) Au(111), and (**C**) Au(100) single-crystal substrates. In (A), the (200) planes of the (110)-oriented film and substrate were selected by tilting the sample 45°. In (B), the (220) planes of the (111)-oriented film and substrate were selected by tilting the sample 35.25°. In (C), the (220) planes of the (111)-oriented film were selected by tilting the sample 35.25°, and the (220) planes of the (100)-oriented substrate were selected by tilting the sample 45°. The x-ray radiation was Cu Kα. The δ-Bi$_2$O$_3$ peaks (purple) are rotated in relation to the Au peaks (yellow) in all three cases. The rotation is 90° on Au(110), ±8.9° on Au(111), and 0° and ±30° on Au(110).

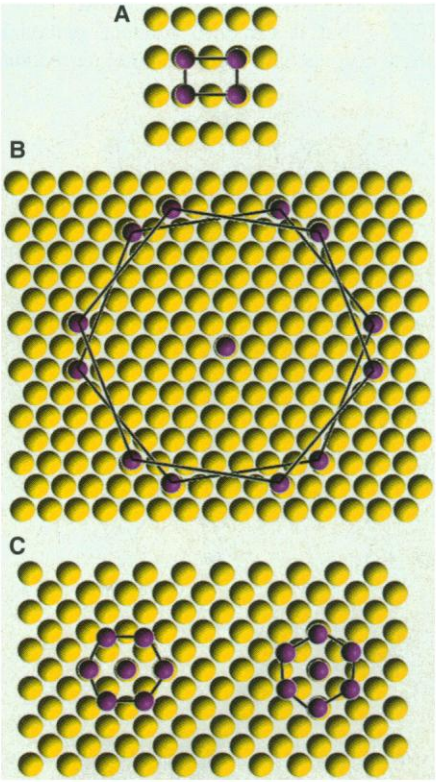

Fig. 4. Interface models for epitaxial growth of δ-Bi$_2$O$_3$ on (**A**) Au(110), (**B**) Au(111), and (**C**) Au(100). The Au substrate atoms are yellow, and the Bi atoms of δ-Bi$_2$O$_3$ are purple. The solid lines indicate unit meshes of the δ-Bi$_2$O$_3$ surface nets. The δ-Bi$_2$O$_3$ film is rotated 90° in relation to Au(110), ±8.9° in relation to Au(111), and 0° and ±30° in relation to Au(100). The (1 × 1) Bi$_2$O$_3$(110)[110]//(2 × 1)Au(110)[100] and Bi$_2$O$_3$(111)[121]//Au(100)[100] coincidence lattices in (A) and (C) both have a mismatch of −4.2%, and the (4 × 4)Bi$_2$O$_3$(111)//($\sqrt{31}$ × $\sqrt{31}$ *R*8.9°) Au(111) coincidence lattice in (B) has a mismatch of −2.7%.

(*24*). Single-crystal films are essential for devices based on superconductor, giant magnetoresistance, thermionic, piezoelectric, and ferroelectric metal oxides because the intrinsic properties of the material, rather than its grain boundaries, can be exploited. The most active crystallographic orientation can also be selected. Our results show that epitaxy can be achieved even for systems with very high lattice mismatch, and they provide a method for producing other nonequilibrium phases that cannot be accessed by traditional thermal processing.

References and Notes

1. J. A. Switzer, M. J. Shane, R. J. Phillips, *Science* **247**, 444 (1990).
2. J. A. Switzer, R. P. Raffaelle, R. J. Phillips, C.-J. Hung, T. D. Golden, *ibid.* **258**, 1918 (1992).
3. J. A. Switzer *et al.*, *ibid.* **264**, 1573 (1994).
4. R. J. Phillips, T. D. Golden, M. G. Shumsky, E. W. Bohannan, J. A. Switzer, *Chem. Mater.* **9**, 1670 (1997).
5. J. A. Switzer *et al.*, *J. Am. Chem. Soc.* **120**, 3530 (1998).
6. J. A. Switzer, B. M. Maune, E. R. Raub, E. W. Bohannan, *J. Phys. Chem. B* **103**, 395 (1999).
7. P. Shuk, H.-D. Wiemhöfer, U. Guth, W. Göpel, M. Greenblatt, *Solid State Ionics* **89**, 179 (1996).
8. A. M. Azad, S. Larose, S. A. Akbar, *J. Mater. Sci.* **29**, 4135 (1994).
9. For a compilation of work on UPD metals on single-crystal surfaces, see E. Budevski, G. Staikov, W. J. Lorenz, *Electrochemical Phase Formation and Growth: An Introduction to the Initial Stages of Metal Deposition* (Wiley-VCH, Weinheim, Germany, 1996), pp. 41–146; *ibid.*, pp. 317–322.
10. ———, *ibid.*, pp. 201–260.
11. T. P. Moffat, *J. Electrochem. Soc.* **142**, 3767 (1995).
12. D. Lincot *et al.*, *Appl. Phys. Lett.* **67**, 2355 (1995).
13. Y. Golan, J. L. Huchison, I. Rubinstein, G. Hodes, *Adv. Mater.* **8**, 631 (1996).
14. G. S. Hsiao, M. G. Anderson, S. Gorer, D. Harris, R. M. Penner, *J. Am. Chem. Soc.* **119**, 1439 (1997).
15. H. A. Harwig, *Z. Anorg. Allg. Chem.* **444**, 151 (1978).
16. P. D. Battle, C. R. A. Catlow, J. Drennan, A. D. Murray, *J. Phys. C. Solid State Phys.* **16**, L561 (1983).
17. K. Koto, K. Suda, N. Ishizawa, H. Maeda, *Solid State Ionics* **72**, 79 (1994).
18. L. E. Depero and L. Sangaletti, *J. Solid State Chem.* **122**, 439 (1996).
19. J. A. Switzer, *Ceram. Bull.* **66**, 1521 (1987).
20. R. A. Van Leeuwen, C.-J. Hung, D. R. Kammler, J. A. Switzer, *J. Phys. Chem.* **99**, 15247 (1995).
21. B. E. Breyfogle, C.-J. Hung, M. G. Shumsky, J. A. Switzer, *J. Electrochem. Soc.* **143**, 2741 (1996).
22. T. D. Golden *et al.*, *Chem. Mater.* **8**, 2499 (1996).
23. J. A. Switzer *et al.*, *J. Mater. Res.* **13**, 909 (1998).
24. We have shown (J. A. Switzer, M. G. Shumsky, E. W. Bohannan, in preparation) in our laboratory that single-crystal films of cuprous oxide (Cu$_2$O) can also be epitaxially electrodeposited onto single-crystal Au. In this case, the lattice mismatch is only 4.4%, and the Cu$_2$O overlayer is not rotated in relation to the Au substrate.
25. This work was supported by the Office of Naval Research grant N00014-96-1-0984, NSF grants CHE-9816484 and DMR-9704288, and the University of Missouri Research Board.

12 January 1999; accepted 2 March 1999

The Fermionic Hanbury Brown and Twiss Experiment

M. Henny,[1] S. Oberholzer,[1] C. Strunk,[1] T. Heinzel,[2] K. Ensslin,[2] M. Holland,[3] C. Schönenberger[1]*

A Hanbury Brown and Twiss experiment for a beam of electrons has been realized in a two-dimensional electron gas in the quantum Hall regime. A metallic split gate serves as a tunable beam splitter to partition the incident beam into transmitted and reflected partial beams. In the nonequilibrium case the fluctuations in the partial beams are shown to be fully anticorrelated, demonstrating that fermions exclude each other. In equilibrium, the cross-correlation of current fluctuations at two different contacts is also found to be negative and nonzero, provided that a direct transmission exists between the contacts.

Experiments aiming at quantum-statistical properties of radiation fields date back to the 1950s when Hanbury Brown and Twiss determined the size of a radio star by measuring the coherence of the observed radiation with an intensity correlation experiment (*1*). In a follow-up optical tabletop experiment the light of a mercury lamp was partitioned with a beam splitter into a transmitted and reflected beam. The intensity correlation between the two partial beams was found to be positive, demonstrating an enhanced probability for the simultaneous detection of two photons—one in each partial beam (*2*, *3*). This is a generic property for a stream of particles obeying Bose-Einstein statistics, in which the particles tend to bunch in clusters. In contrast, antibunching is expected for fermions, because two indistinguishable fermions must exclude each other by the Pauli principle (Fig. 1). With their experiment Hanbury Brown and Twiss founded the discipline of quantum-statistical measurements, which has led to important developments in quantum optics (*4*). Correlation experiments along the lines of Hanbury Brown and Twiss are today also an important tool in particle physics (*5*).

In the Hanbury Brown and Twiss (HBT) experiment an average over many particles is measured. In general, the time-dependent intensity $I(t)$ of a stream of particles exhibits fluctuations ΔI around the average current $\langle I \rangle$ known as shot noise, which has recently attracted much attention in electrical transport of submicrometer-sized nanostructures (*6*, *7*). Shot noise is due to the fluctuation ΔN of the number of particles N detected during a certain time interval. For a classical stream obeying Poisson statistics $\langle (\Delta N)^2 \rangle = \langle N \rangle$, whereas for a stream of bosons obeying Bose-Einstein statistics $\langle (\Delta N)^2 \rangle$ is larger, that is, super-Poissonian. In contrast, for degenerate fermions the stream is noiseless, indicating the complete absence of fluctuations in the occupation of states according to the Pauli principle. Suppression of electrical-current noise of this origin has recently been found in electrical measurements on quantum-point

---

[1] Institute of Physics, University of Basel, Klingelbergstrasse 82, CH-4056 Basel, Switzerland. [2] Solid State Physics Laboratory, ETH Zürich, CH-8093, Switzerland. [3] Department of Electronics, University of Glasgow, Glasgow G12 8QQ, UK.

*To whom correspondence should be addressed: E-mail: schonenberg@ubaclu.unibas.ch